# Photomodulated reflectance study of In$_x$Ga$_{1-x}$As/GaAs/AlAs microcavity vertical-cavity surface emitting laser structures in the weak-coupling regime: The cavity/ground-state-exciton resonance

P. J. Klar, G. Rowland, P. J. S. Thomas, A. Onischenko, T. E. Sale, and T. J. C. Hosea*
*School of Physical Sciences, University of Surrey, Guildford GU2 5XH, Surrey, United Kingdom*

R. Grey
*EPSRC III-V Central Facility, University of Sheffield, Mappin Street, Sheffield S1 3JD, United Kingdom*
(Received 20 January 1998; revised manuscript received 19 October 1998)

Two InGaAs/GaAs/AlAs vertical-cavity surface emitting laser (VCSEL) structures have been studied by conventional reflectance (R) and photomodulated reflectance (PR) spectroscopies at ~300 K and ~80 K. Growth variations across the samples (<2%) give rise to smooth changes in the cavity mode energy so that it can be tuned through the position of resonance with the quantum well (QW) ground-state exciton, by varying the position of measurement. The R spectra show the cavity mode but at best only a weak excitonic feature. In contrast, the PR shows two prominent and distinct signals, and there is a strong enhancement (up to 40 times) at resonance. A theory has been developed for the PR modulation of the coupled cavity and exciton modes, based on energy dependent Seraphin coefficients. This was used to fit all the PR spectra simultaneously in each complete set of position dependent measurements, using seven parameters, only one of which, the cavity mode energy, varied significantly. The resulting cavity mode and excitonic energies do not clearly show an anti-crossing behavior near resonance, implying only a weak exciton-cavity coupling. The ability of PR to detect, in a nondestructive manner, both the cavity and exciton modes, and the extent to which they are in resonance, suggests it could be extremely useful in the characterization of VCSEL structures near their operating temperature. [S0163-1829(99)01904-9]

## I. INTRODUCTION

There has been a great deal of recent interest in the interaction between optical modes and excitonic states in two-dimensional (2D) systems such as quantum wells (QWs) in semiconductor microcavities. In contrast to the bulk case, such exciton polaritons are not stable in 2D because the QW exciton momentum is only conserved in the plane of the QW, allowing the dipole-allowed exciton to couple to a continuum of light modes. However, this problem can be overcome by embedding the QW in a high finesse Fabry-Pérot planar optical cavity, which condenses the continuum to a single optical mode. If the energy of this mode is in resonance with that of a QW excitonic transition, stable exciton polaritons can be formed. By analogy with the atom-cavity system, the resultant level repulsion and anticrossing behavior between the exciton and cavity modes is referred to as Rabi splitting. This may be defined as the energy separation of the two modes, which reaches a certain minimum value when they are in resonance.

Theoretical studies show that the occurrence, as well as the magnitude, of the Rabi splitting in 2D semiconductor systems depends strongly on the QW/cavity coupling,[1–3] again all by analogy with the atom-cavity system (see, e.g., Ref. 4). There are two coupling regimes which can be crudely defined by comparing the energy separation (Rabi splitting) of the cavity mode and exciton, to their half-widths at half maximum (HWHM): (i) strong coupling, where the Rabi splitting exceeds the sum of the HWHMs; (ii) weak coupling, where the opposite is true and where Rabi splitting

may not be observable. The transition between the two regimes is continuous.[1,5,6] Coupling can be increased in several ways: introducing more QW's into the cavity, positioning the QW's nearer the antinodes of the cavity mode standing-wave field, increasing the QW exciton oscillator strength using magnetic fields or low temperatures, increasing the mirror reflectance, i.e., the cavity finesse, or decreasing the cavity length.

Most experimental studies of light-matter interactions in QW exciton cavity systems have been performed in the strong-coupling regime on quantum microcavities (QMC's).[5–14] These are similar to vertical-cavity surface emitting lasers (VCSEL's) in that both are Fabry-Pérot structures consisting of two high reflectance distributed Bragg reflectors (DBR's), sandwiching a short cavity, in which the QW's lie at the antinodes of the cavity mode whose energy matches that of the QW ground-state transition. In general, however, VCSEL structures are not designed to maximize the strength of the exciton cavity coupling, but rather to minimize the current for a given output lasing power of the actual device.[15,16] Generally, this different design maxim means that, in comparison to QMC's, there are fewer QW's and the output DBR has a smaller reflectance. Thus, one may anticipate that in VCSEL's the QW exciton cavity interaction lies in the weak-coupling regime. In such low-Q microcavities, the cavity polaritons are not radiatively stable, but decay into photons propagating external to the cavity.

Most experimental studies of Rabi splitting in QMC's use conventional reflectance (R) spectroscopy,[5–12] usually below ~150 K since excitonic oscillator strengths are increased at

low temperatures, leading to a stronger exciton cavity coupling.[11] Since real VCSEL's are generally designed to operate near room temperature, the cavity exciton resonance also occurs around 300 K. Unfortunately, previous reflectance studies on VCSEL's have shown that it is very difficult to observe clear excitonic signals in the complex R spectra near 300 K, even in the region of the flat high-reflectance stop band,[17–21] and there is only one report of Rabi splitting at ~300 K.[11] This can be overcome using modulation spectroscopy, in particular photomodulated reflectance (PR), where clear features related to both the cavity mode and QW transitions have been observed in VCSEL structures at room temperature.[20,21]

However, to analyze such PR spectra fully, it is essential to be able to fit them with an appropriate line shape model, especially when several oscillatory features overlap, as is the case when the exciton and cavity modes are near to resonance. The theory of PR line shapes is well developed for excitonic transitions in bulk and heterostructure semiconductors (see, e.g., Ref. 22), but this is not appropriate for the PR signal of the VCSEL cavity mode since this a nonexcitonic feature arising from optical interference between the various interfaces in the structure. So far, the mechanism giving rise to a cavity mode PR signal has been explained only qualitatively in terms of a laser induced modulation of the complex refractive index.[20,21]

Here we present a detailed PR study of resonances between the cavity mode and QW excitons, particularly the ground-state exciton, in InGaAs/GaAs/AlAs VCSEL structures. We also focus on developing a model for the PR line shape of these signals. In the following paper,[23] we describe a method of using PR to monitor the higher-order QW excitonic transitions in the same structures, and analyze the PR signals of these resonances using this line shape model.

## II. EXPERIMENTAL DETAILS

Two InGaAs/GaAs/AlAs VCSEL samples designed for a working wavelength of $\lambda = 1~\mu m$ were grown by solid source molecular beam epitaxy on (100) GaAs substrates.[21,24] The first sample, RMB1048, consists of a GaAs cavity, of optical length $\sim\lambda$, with a nominally 85 Å-thick $In_{0.23}Ga_{0.77}As$ QW located at the antinode of the standing wave at the cavity center. The cavity is embedded between two AlAs/GaAs DBR's with stepped interfaces. The top, Be-doped ($p$-type), DBR has 16.5 periods, while the bottom, Si-doped ($n$-type) DBR, has 28.5 periods. Both DBR's have doping levels of $1.0 \times 10^{18}~cm^{-3}$ in the AlAs and GaAs layers and $5 \times 10^{18}~cm^{-3}$ in the stepped interface regions. The second sample, RMB627, is of a different design. It has a GaAs cavity, of optical length $\sim 2\lambda$, with an 85 Å $In_{0.22}Ga_{0.78}As$ QW at each of the three antinodes. The top and bottom DBR's consist of 14.5 and 23.5 AlAs/GaAs periods, respectively. Otherwise, the structure of the DBR's is comparable to that of RMB 1048. The QW's in both samples are compressively strained. Therefore, the ground-state QW transition is the $e1hh1$ exciton formed by the lowest confined electron ($e1$) and highest confined heavy-hole ($hh1$) states. While in RMB627 the QW has an In composition close to the nominal $x=22\%$, in RMB1048 a calibration error resulted in $x=28\%$ so that the $e1hh1$ transition is

about 50 meV lower in energy than the cavity mode at room temperature.[21] Hence, while the resonance between the $e1hh1$ exciton and the cavity mode occurs near 300 K in RMB627, in RMB1048 cooling to ~80 K is necessary. Furthermore, slight fluctuations in growth conditions led to thickness variations of $<\sim 2\%$ over the full width of the wafers. While this does not significantly affect the energy of the ground-state transition in the relatively wide QW's, it does give rise to a significant, though smooth, variation in the energy of the cavity mode across the samples.[21] This was particularly convenient for the present study as it meant that the degree of overlap between the cavity and exciton modes could be varied by probing different regions of the wafers.

The PR and R experiments were carried out with the probe light at normal incidence using a conventional arrangement described in detail elsewhere.[21] Modulation was provided by a chopped (333 Hz), 0.8 mW HeNe laser ($\lambda = 632.8$ nm) which has a penetration depth in the present samples of ~0.6 $\mu m$. Calculations show that, at the depth of the cavity (~2.9 $\mu m$ in RMB1048) the laser power has attenuated to ~6 $\mu W$, which is still evidently enough to modulate the QW's. The spectral resolution was ~1.5 meV (FWHM). In order to change the probe position on the samples, the sample mount, or alternatively a nitrogen cryostat, was attached to a translational stage equipped with a micrometer calibrated in millimeters.

## III. EXPERIMENTAL RESULTS

Figure 1 depicts the normalized R spectra for RMB1048 at ~80 K and RMB627 at ~300 K in the spectral region near the cavity mode/$e1hh1$ exciton resonance, as a function of probe beam position. This was moved in a straight line, along the direction of maximum change in the samples, the corresponding readings of the translational stage micrometer being shown (in mm) in Fig. 1. Both sets of spectra show that the energy of the cavity dip shifts smoothly with position. The energy of the $e1hh1$ exciton, obtained subsequently by PR, is also shown in Fig. 1, at ~1.230 eV for RMB1048 and ~1.222 eV for RMB627. However, there are no clear features in R near the QW transition for RMB627, though a weak dip is visible for RMB1048, especially when the cavity mode lies below the $e1hh1$ transition. This is probably due to the increase in oscillator strength of the $e1hh1$ exciton for RMB1048 at 80 K. However, in both sets of spectra, some indication of the $e1hh1$ transition energy can be gleaned from a change in depth of the cavity dip with position; the dip is shallow when its energy is well below $e1hh1$, but increases in depth, by about five times, when it is near or above $e1hh1$. In RMB1048, but not so much in RMB627, the cavity dip is also deepest when it is near resonance. A characteristic observation of the Rabi splitting effect is an anticrossing, level repulsion behavior near resonance. This is manifested by a doubling in the Fabry-Pérot dip structure in R; as resonance is approached, the energies of the dips move closer, reaching a certain minimum value (the Rabi splitting) at which point the depth of the dips become comparable.[5–12] This is not observed here in either sample, even when the spectral resolution was improved to ~0.5 meV, suggesting that, as expected, both VCSEL samples lie in the weak-coupling regime.
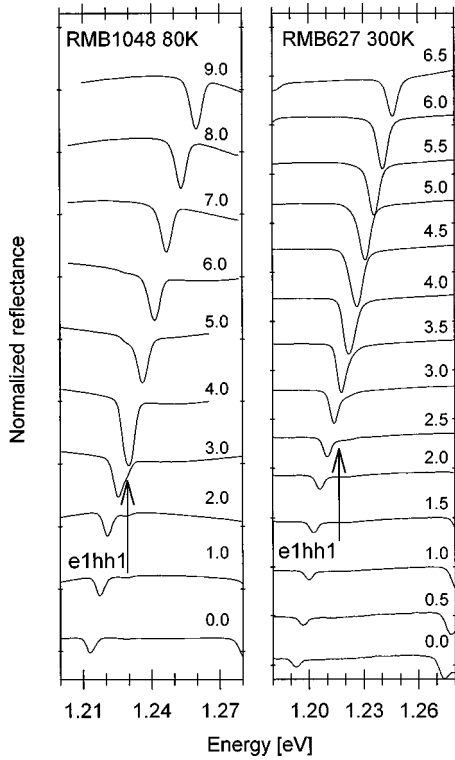
FIG. 1. Normalized R spectra at normal incidence in the vicinity of the high reflectance stop band for VCSEL structures RMB1048 at ~80 K (left) and RMB627 at ~300 K (right), as a function of position of the probe beam on the samples, indicated on the right by the micrometer setting (in mm). The high- and low-energy edges of the stop band are visible at the low and high micrometer settings. The baselines are offset vertically by increments of 0.45 and 0.7 for RMB1048 and RMB627, respectively. The energy of the ground-state QW transition $e1hh1$ (obtained subsequently by PR—see Figs. 2 and 3), is indicated by the vertical arrows.

Figures 2 and 3 show the corresponding PR spectra for RMB1048 and RMB627, respectively. Also shown are fits to the experimental data (for discussion of these, and the line shape model, see Sec. IV). Both sets of PR spectra clearly show two features which can be assigned to the cavity mode and the $e1hh1$ exciton. The $e1hh1$ transition energy (1.230 eV for RMB1048 at 80 K and 1.222 eV for RMB627 at 300 K) does not depend noticeably on probe position, but, in agreement with the R spectra, the cavity feature increases in energy with increasing micrometer setting, so crossing the energy of the $e1hh1$ exciton. For RMB1048, the resonance occurs near the 4.0 mm position, while for RMB627, it occurs near 3.5 mm. From the scaling factor indicated on the left of Figs. 2 and 3, it may be seen that the PR signal strength is enhanced at resonance, by factors of 25 and 40, for RMB1048 and RMB627, respectively. Although the PR signals of $e1hh1$ exciton and cavity mode are clearly distinguishable when they do not overlap, a complicated line shape arises when they do. Thus, without line shape modelling, it is difficult to decide from the PR spectra whether the modes cross, and are thus in the weak-coupling regime, or whether they exhibit the anticrossing behavior characteristic of strong coupling.
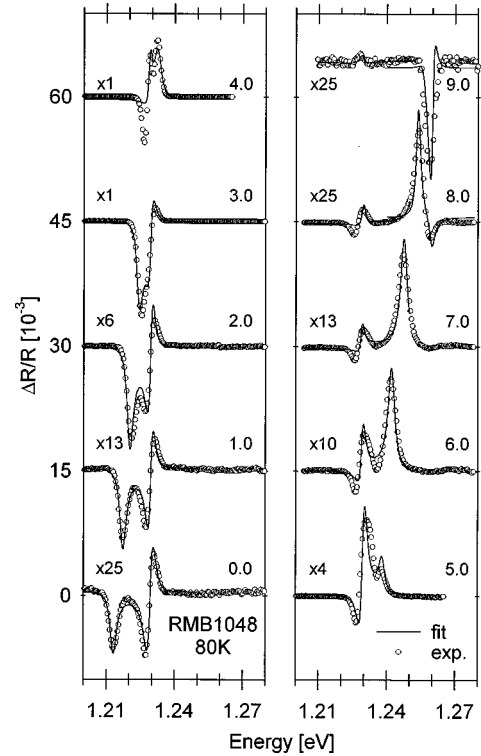


FIG. 2. Position-dependent PR spectra (open circles; only every second data point plotted) for RMB1048 at ~80 K, corresponding to the R spectra on the left of Fig. 1. By varying the position of the probe beam on the sample, indicated on the right (in mm), the cavity mode was tuned through resonance with the $e1hh1$ transition at 1.230 eV; this occurs near the 4.0 mm position. The baselines of the spectra are offset by increments of $1.5 \times 10^{-2}$ units and are scaled by factors shown on the left. The lines represent least-squares fits using Eqs. (1)–(4).

## IV. THEORY OF THE PR LINE SHAPES

PR is usually considered as a variant of electroreflectance spectroscopy (for a review see, e.g., Ref. 22), and the signal conventionally expressed by

$$\frac{\Delta R}{R}(E) = \alpha(E)\Delta\varepsilon_1(E) + \beta(E)\Delta\varepsilon_2(E), \tag{1}$$

where $\Delta\varepsilon_1$ and $\Delta\varepsilon_2$ are the real and imaginary parts, respectively, of the modulation induced changes in the complex dielectric function $\varepsilon$. The Seraphin coefficients[25] are defined as

$$\alpha(E) = \frac{1}{R(E)}\left(\frac{\partial R(E)}{\partial\varepsilon_1(E)}\right)\bigg|_E, \quad \beta(E) = \frac{1}{R(E)}\left(\frac{\partial R(E)}{\partial\varepsilon_2(E)}\right)\bigg|_E. \tag{2}$$

In a bulk semiconductor, $\alpha$ and $\beta$ may be obtained at a given angle of incidence or polarization by performing the derivatives in Eq. (2) analytically, using an expression for R obtained from Fresnel's equations.[25,26] In heterostructures, such as single or multiple QW's, the PR spectrum is analyzed in a similar way—it can be considered as a superposition of line shape contributions of the different layers, each contribution being calculated according to Eqs. (1) and (2). The R spectrum can be calculated at arbitrary angle of incidence and
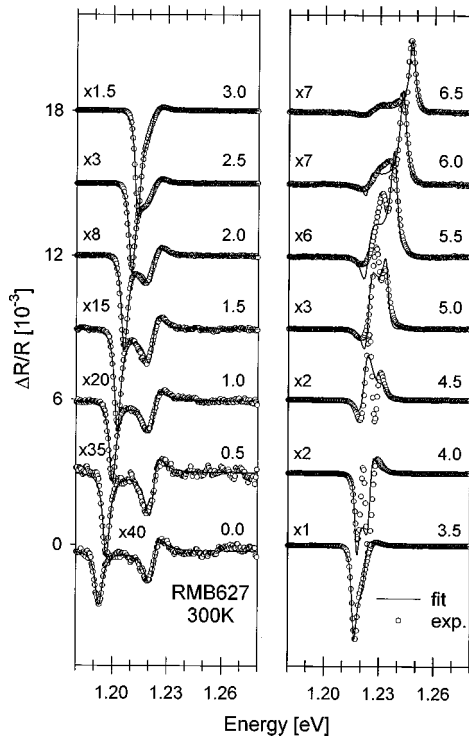
FIG. 3. Position dependent PR spectra (open circles; only every second data point plotted) for RMB627 at ~300 K, corresponding to the R spectra on the right of Fig. 1. By varying the position of the probe beam on the sample, indicated on the right (in mm), the cavity mode was tuned through resonance with the $e1hh1$ transition at 1.222 eV; this occurs near the 3.5 mm position. The baselines of the spectra are offset by increments of $3.0 \times 10^{-3}$ units and are scaled by factors shown on the left. The lines represent least-squares fits using Eqs. (1)–(4).

polarization using a Jones matrix approach,[21] where the optical properties of the layers are usually approximated by the bulk values. This does not generally yield an analytically differentiable expression for R, but $\alpha$ and $\beta$ can be obtained by numerical differentiation.[27,28] In general, one finds that $\alpha$ and $\beta$ vary smoothly as a function of photon energy $E$, for both bulk semiconductors and individual layers in a heterostructure, and are, therefore, usually assumed, often tacitly, to be constant in the vicinity of the critical points of the band structure, or near excitonic and electronic transitions.[29–31] In contrast, $\Delta\varepsilon_1$ and $\Delta\varepsilon_2$ exhibit sharp derivativelike features near the critical points and so dominate the PR line shapes. Thus the influence of $\alpha$ and $\beta$ on the PR line shape is generally of secondary importance; they alter the ratio of the contributions of $\Delta\varepsilon_1$ and $\Delta\varepsilon_2$ when the angle of incidence, or polarization, is varied,[26] and thus provide the phase information in the PR spectrum.[27,28]

For bulk semiconductors, and most simple heterostructures, the R spectrum is determined primarily by electronic and excitonic band structures. In contrast, in the very complex structure of a VCSEL, the R spectrum is deliberately engineered to produce the high reflectance stop band with a sharp cavity dip in its center, and interference fringes on either side—excitonic and electronic features generally play a minor role. One might anticipate that such prominent, though nonexcitonic, features in the R spectrum may have counterparts in the corresponding PR spectrum.
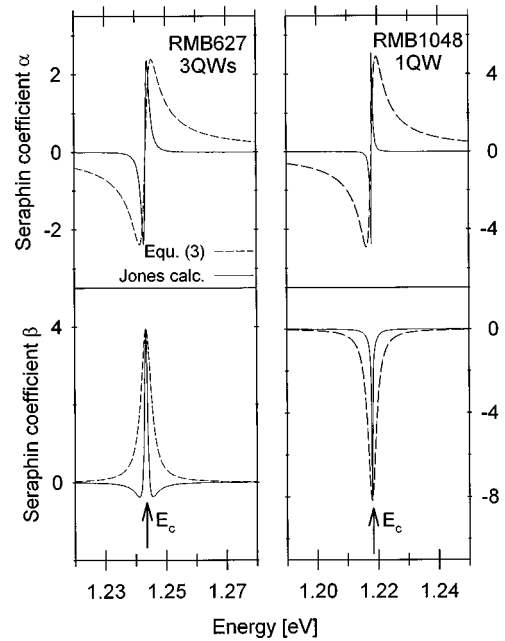


FIG. 4. Seraphin coefficients $\alpha$ and $\beta$ for the three QW layers of RMB627 (left) and the single QW layer of RMB1048 (right) in the vicinity of the cavity mode energy $E_c$. As explained in the text, the solid lines are calculated numerically from the Jones matrix approach, while the dashed lines are derived using the empirical line shape model for the Seraphin coefficients of Eq. (3).

Here, we confirm that such PR signals do indeed arise in VCSEL's, not due to any prominent features in $\Delta\varepsilon_1$ or $\Delta\varepsilon_2$, but rather because $\alpha$ and $\beta$ can no longer be considered as slowly varying functions of energy. The theoretical R spectrum was first calculated using Jones matrices, which take account of all reflections in the multilayer structure.[21] The data for the complex dielectric function of each layer were taken from published bulk values. The Seraphin coefficients of the QW layers in the samples RMB1048 and RMB627 were then calculated in the vicinity of the cavity dip by performing the derivatives in Eq. (2) numerically.[27] The full curves in Fig. 4 show the results for $\alpha$ and $\beta$ (the dashed curves are explained in Sec. V), which, for RMB1048, come from numerically differentiating R with respect to the $\varepsilon$ of the single InGaAs QW, while for RMB627 the derivative was performed with respect to the $\varepsilon$ of all three QW's.

Near the energy of the cavity dip, these calculations all exhibit a sharp feature whose line shape can be qualitatively explained. For RMB1048, with the single QW, the dispersionlike line shape of $\alpha$ ($\sim \partial R/\partial\varepsilon_1$) reflects the change in energy position of the cavity dip, due to the modulation of the refractive index ($\sim \sqrt{\varepsilon_1}$), and thus optical length, of the cavity. The absorptionlike line shape of $\beta$ ($\sim \partial R/\partial\varepsilon_2$) arises from changes in the depth of the dip due to the modulation of the QW absorption ($\sim \varepsilon_2$). While the calculated $\alpha$ for RMB627 is very similar, its $\beta$ is different—the main peak is positive, rather than negative, and there are small negative side lobes. This difference was thought to be due to the fact that RMB627 has three QW's, which produces extra optical interference effects. This was confirmed by recalculating $\beta$ for the RMB627 structure with the number of QW's reduced to one; it was found that the resulting line shape for $\beta$ became virtually identical to that of RMB1048.

TABLE I. Mean values and standard deviations of six of the fitting parameters of the PR line shape model defined by Eqs. (1)–(4), as obtained from fitting the individual sets of position-dependent spectra for RMB1048 (Fig. 2) and RMB627 (Fig. 3). These parameters can be assumed to be virtually constant throughout each set, whereas the seventh parameter $E_c$ depends on the probe beam position on the samples.

| Sample | $I_1$ [$10^{-10}$ (eV)$^3$] | $I_2$ [$10^{-10}$ (eV)$^3$] | $\Gamma_c$ [meV] | $\Gamma_{qw}$ [meV] | $E_{qw}$ [eV] | $\theta$ [deg] |
|---|---|---|---|---|---|---|
| RMB627 | $0.3 \pm 0.4$ | $-4.2 \pm 1.2$ | $2.0 \pm 0.2$ | $4.0 \pm 0.5$ | $1.2224 \pm 0.0008$ | $2° \pm 20°$ |
| RMB1048 | $0.5 \pm 0.4$ | $4.4 \pm 1.8$ | $1.7 \pm 0.1$ | $1.8 \pm 0.3$ | $1.2294 \pm 0.0002$ | $7° \pm 28°$ |

Despite these differences, the line shapes of the Seraphin coefficients of the QW layers of both samples in Fig. 4 can, to a reasonable approximation, be described empirically by the real and imaginary parts of a complex Lorentzian:

$$\alpha(E) = I_1 \frac{(E - E_c)}{(E - E_c)^2 + \Gamma_c^2}, \quad \beta(E) = I_2 \frac{\Gamma_c}{(E - E_c)^2 + \Gamma_c^2}, \tag{3}$$

where $E_c$ and $\Gamma_c$ denote the energy position and half-width, and $I_1$ and $I_2$ the amplitudes.

The line shapes of $\Delta\varepsilon_1$ and $\Delta\varepsilon_2$ in Eq. (1) are associated with the allowed QW $e1hh1$ excitonic transition. A conventional description was assumed, given by the linear combination of the first derivatives of a complex Lorentzian with respect to energy position and linewidth, as discussed in detail elsewhere:[32]

$$\Delta\varepsilon_1(E) = \frac{(E - E_{qw})^2 - \Gamma_{qw}^2}{[(E - E_{qw})^2 + \Gamma_{qw}^2]^2} \cos\theta$$
$$+ \frac{2\Gamma_{qw}(E - E_{qw})}{[(E - E_{qw})^2 + \Gamma_{qw}^2]^2} \sin\theta,$$

$$\Delta\varepsilon_2(E) = \frac{(E - E_{qw})^2 - \Gamma_{qw}^2}{[(E - E_{qw})^2 + \Gamma_{qw}^2]^2} \sin\theta$$
$$- \frac{2\Gamma_{qw}(E - E_{qw})}{[(E - E_{qw})^2 + \Gamma_{qw}^2]^2} \cos\theta, \tag{4}$$

where $E_{qw}$ is the energy position of the exciton and $\Gamma_{qw}$ its HWHM. The angle $\theta$ accounts for the degree of mixing of the two types of first derivative; $\theta = 0°$ and $\theta = 90°$ correspond to the derivative with respect to purely $E_{qw}$ and $\Gamma_{qw}$, respectively. No amplitude parameter is included in Eq. (4), since this is accounted for by Eq. (3). It might be noted that Eq. (4) is formally equivalent to Aspnes's differential PR fitting function for excitons.[33]

The PR line shape model to describe the two oscillators (cavity mode and exciton) is thus given by Eqs. (1)–(4). It requires seven fitting parameters ($I_1, I_2, E_c, \Gamma_c, E_{qw}, \Gamma_{qw}$, and $\theta$), comparable in quantity to that of conventional PR models to describe, say, two excitonic oscillators (usually three to four parameters for each). However, there is a crucial difference: while in a conventional two-oscillator model the two line shapes are summed, in our new model two oscillators are multiplied together.

As the cavity and exciton oscillators move through the position of resonance, our model has the following interesting properties: (i) Away from resonance, i.e., $|E_{qw} - E_c| > 2|\Gamma_{qw} + \Gamma_c|$, the PR signal of the cavity mode near $E_c$ arises solely from the sharp feature in $\alpha$ and $\beta$ multiplied by the slowly varying tail of the $\Delta\varepsilon$ exciton signal at $E_{qw}$, and vice versa for the PR signal of the exciton, so the result is not very dissimilar to that of a conventional superposition of two excitonic oscillators. (ii) More importantly, however, close to the cavity exciton resonance, i.e., $|E_{qw} - E_c| < 2|\Gamma_{qw} + \Gamma_c|$, the differences to a conventional model become much more apparent; the multiplication of $\Delta\varepsilon_1$ and $\Delta\varepsilon_2$ by $\alpha$ and $\beta$ gives rise to a strong nonlinear enhancement of the PR signal.

This line shape model for the cavity exciton resonance does not account for a mixing of the two modes (i.e., polariton formation) and is, therefore, strictly valid only in the weak-coupling regime. However, it may still be useful even for strong coupling, yielding approximate Rabi splitting values.

## V. RESULTS AND DISCUSSION

The PR spectra of the cavity mode/$e1hh1$ exciton resonance were least-squares fitted using our new line shape model, as shown in Figs. 2 and 3 for RMB1048 and RMB627, respectively. Clearly, the quality of the fits is, in general, very satisfactory, with the model reproducing both the line shape at resonance and the accompanying large enhancement of the signal strength (by 25 and 40 times, for RMB1048 and RMB627, respectively).

Initially, all seven fitting parameters were permitted to vary freely. However, it was found that, apart from $E_c$, these did not change significantly throughout either set of PR spectra and they could be effectively held fixed at their mean values. These, and standard deviations, are given in Table I, which can be summarized as follows: (i) The standard deviations in $E_{qw}$, $\Gamma_{qw}$, and $\Gamma_c$ are all less than 1 meV. (ii) $I_2$ is an order of magnitude larger than $I_1$, showing that 90% of the PR signal arises from the product of $\beta$ and $\Delta\varepsilon_2$, and only 10% from $\alpha$ and $\Delta\varepsilon_1$. The standard deviations of $I_1$ and $I_2$ are $\sim$100% and $\sim$30%, the former being expected because of the small contribution to the signal scaled by $I_1$. Thus, the variations in $I_1$ and $I_2$ are small in comparison to the enhancement observed in PR signal strength, so confirming that this latter fact is a completely natural feature of the new line shape model. (iii) The derivative mixing parameter $\theta$ has mean values close to 0° with a standard deviation of about $\pm25°$. Hence, about 70% or more of the modulation of $\varepsilon$ comes from the energy derivative of the complex Lorentzian, in agreement with previous studies of QW samples.[34]

We may compare the Seraphin coefficients derived earlier in the Jones matrix theory with the empirical line shapes for

$\alpha$ and $\beta$ given by Eq. (3). These are shown as the dashed curves in Fig. 4. The $\Gamma_c$ used is the mean value from the fitting, but $E_c$, and an arbitrary intensity scaling factor, are chosen to facilitate comparison with the Jones calculations. It can be seen that the empirical curves are broader than those calculated theoretically. However, this is expected and reflects the fact that the actual structure deviates significantly from nominal, in that the observed cavity dip (see R spectra of Fig. 1) has a much lower apparent finesse than is calculated theoretically:[21] the broader empirical Seraphin coefficients simply reflect the need for a realistic and appropriate broadening in fitting of the cavity mode feature in the PR spectra of Figs. 2 and 3. Furthermore, the interference side lobes in $\beta$ for RMB627 cannot, of course, be reproduced by the simplified empirical model of Eq. (3).

These differences between the theoretical and empirical line shapes of the Seraphin coefficients can in part explain the slight discrepancies between the experimental PR spectra and fits in Figs. 2 and 3. In the PR spectra of RMB627 (Fig. 3), the fits very accurately reproduce the experimental line shapes up to the 3.5 mm position. However, two discrepancies occur at higher micrometer settings. First, in the spectra at 4.0 and 4.5 mm (i.e., close to resonance, with $E_{qw} \approx E_c$) a sharp extremum feature is not well described. Secondly, for 5.5 and 6.0 mm (i.e., off resonance, with $E_{qw} < E_c$), a broad shoulder on the high-energy side of the $e1hh1$ exciton is not well represented. The first discrepancy is probably caused by the neglect of the side lobes in $\beta$ in Eq. (2) (see Fig. 4); although these lobes are weak, the significant changes which occur in the magnitude and sign of $\Delta\varepsilon_2$ around $E_{qw}$ mean that the PR signal could be strongly enhanced in the vicinity of the lobes, perhaps causing the additional extremum observed in the 4.0 and 4.5 mm spectra. Away from resonance, $\Delta\varepsilon_2$ can be considered as roughly energy independent and the presence of the side lobes in $\beta$ should not be significant. The second discrepancy is probably caused by the fact that the $e1hh1$ transition is not purely excitonic at 300 K so that the Lorentzian model for the complex dielectric function [Eq. (4)] is not strictly appropriate.

In the PR spectra of RMB1048 (Fig. 2), the overall quality of the fits is somewhat better than for RMB627, probably because Eqs. (3) and (4) are now more appropriate, in the former case because no side lobes occur in the Jones calculation of $\beta$ (see Fig. 4), and in the latter because the $e1hh1$ transition is more closely excitonic at $\sim$80 K. However, slight differences may still exist between the empirical and real Seraphin coefficients and, again, these would be enhanced in the vicinity of the resonance, as is perhaps observed in the PR spectrum at 4.0 mm. An interesting effect occurs in moving from 8.0–9.0 mm where the sign of the cavity PR feature switches. We believe this is caused by the cavity mode approaching a higher-order QW transition whose contribution to $\Delta\varepsilon$ starts to dominate, but which happens to have an opposite sign to that of the $e1hh1$ transition. This was accounted for in the fit of these two PR spectra by allowing for a resonance with a second $\Delta\varepsilon$ feature. This yielded an energy position of 1.260 eV (HWHM $\approx$ 2 meV), indicating that it is due to the $e1hh2$ QW transition (at 80 K). Such higher-order resonances are studied in more detail in the following paper.[23]

Figures 5 and 6 summarize the results of the R and PR
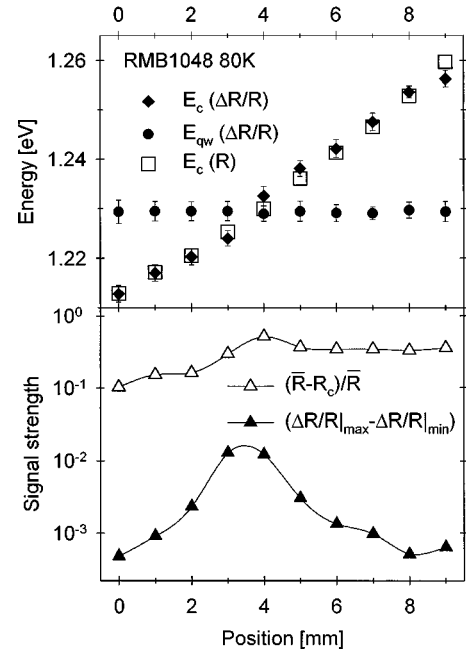


FIG. 5. Summary of the results from the position dependent R and PR spectra of RMB1048 at $\sim$80 K. Upper graph: the solid circles and solid diamonds represent the energies of the $e1hh1$ exciton $E_{qw}$ and cavity mode $E_c$, respectively, obtained by fitting the PR with Eqs. (1)–(4); the open squares represent the cavity mode energies deduced from the minima in the R spectra. The bars on the PR data indicate the HWHM values obtained in the fits, not error bars. Lower graph: dependence of the signal strength on probe position, according to the empirical definitions given in the text.

experiments and the fitting of the PR spectra as a function of position. The upper graph shows the fitted $e1hh1$ PR energy, and the cavity mode energy obtained from both the PR and corresponding R spectra, which are in good agreement. The figures also show the HWHM's obtained in the fitting which are intended as a guide to the broadening of the two PR signals, rather than error bars. The lower graph shows the dependence on probe position of the signal strength (note logarithmic scale), which we defined empirically as follows: in the R spectra, by the relative depth of the cavity dip and, in the PR spectra, by the difference between the largest positive and negative extrema in $\Delta R/R$.

For RMB1048 (Fig. 5), the cavity mode energy changes roughly linearly with probe position whereas that of $e1hh1$ remains virtually constant. The crossing point occurs near 4.0 mm. Here, the minimum difference in energy of the two modes is $\sim$3.5 meV, which is smaller than the sum of their respective HWHM's ($\Gamma_c + \Gamma_{qw} \approx 4$ meV). Therefore, if a Rabi splitting occurs for RMB1048 it is less than 3.5 meV and may not be resolved. In the lower part of Fig. 5, the strengths of the R and PR signals both show a resonant behavior peaking near the crossing point of 4.0 mm, though the resonance is far more pronounced in the PR.

The situation is similar for RMB627 (Fig. 6). The energy of the exciton hardly changes, while the cavity mode shows a roughly linear behavior with probe position. Only in the vicinity of the crossing point, between 4.0 and 4.5 mm, do the cavity mode energies obtained by fitting the PR deviate
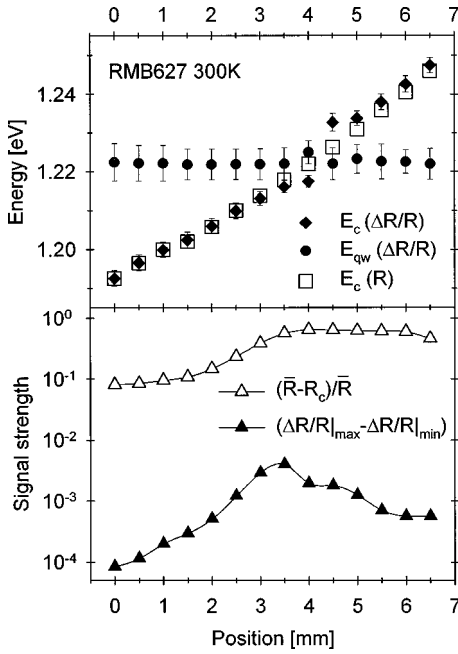
FIG. 6. Summary of the results from the position dependent R and PR spectra of RMB627 at ~300 K. Upper graph: the solid circles and solid diamonds represent the energies of the $e1hh1$ exciton $E_{qw}$ and cavity mode $E_c$, respectively, obtained by fitting the PR with Eqs. (1)–(4); the open squares represent the cavity mode energies deduced from the minima in the R spectra. The bars on the PR data indicate the HWHM values obtained in the fits, not error bars. Lower graph: dependence of the signal strength on probe position, according to the empirical definition given in the text.

noticeably from those obtained from R. However, this is more likely to be caused by the aforementioned problems in the fitting rather than an indication of any anticrossing behavior. Near the crossing point, the minimum difference in energy of the two modes is ~5 meV, which again is smaller than the sum of their respective HWHM's ($\Gamma_c + \Gamma_{qw} \approx 6$ meV). Therefore, if a Rabi splitting occurs for RMB627 it is less than 5 meV and may not be resolved. In the lower part of Fig. 6, the PR signal shows a strong resonance near the crossing point whereas R shows only the onset of a plateau.

These results indicate that both samples are in the weak-coupling regime, in the sense that, if there is a Rabi splitting between the exciton and the cavity mode, it is comparable to, or smaller than, the sum of their HWHM's. This is in agreement with previous studies. For example, Houdré *et al.* reported a Rabi splitting of 4.5 meV at 300 K for a 1.5λ-long GaAs QMC, with six $In_{0.13}Ga_{0.87}As$ QW's, and top and bottom $Al_{0.1}Ga_{0.9}As$/GaAs DBR's with 15 and 19 periods, respectively.[11] Assuming that the cavity of RMB627 with three QW's is comparable to that of Houdré *et al.* and taking into account that the Rabi splitting scales with the square root of the number of QW's in the cavity, one would expect that RMB627 would have a Rabi splitting of ~3 meV at 300 K. Fisher *et al.* observed a Rabi splitting between the cavity mode and $e1hh1$ exciton of 4.6 meV at 80 K, for a sample with a λ-long $Al_{0.2}Ga_{0.8}As$ cavity with three GaAs QW's in the center and with AlAs/$Al_{0.14}Ga_{0.86}As$ DBR's of 20 periods each.[8] Again, assuming that their cavity is comparable to that of RMB1048, the Rabi splitting scales for a single QW to

~2.7 meV. Both these estimates are consistent with our conclusion that any Rabi splitting in RMB627 and RMB1048 is $<\sim 5$ meV and $<\sim 3.5$ meV, respectively.

## VI. SUMMARY AND CONCLUSIONS

We have studied the resonance between the cavity mode and ground-state QW $e1hh1$ exciton in two InGaAs/GaAs/AlAs VCSEL structures, by conventional R spectroscopy, and presented a detailed study of these effects using PR. Due to growth variations, changing the probe position on the sample allows the cavity mode to be tuned through the position of resonance with the exciton. The PR spectra exhibit two strong and prominent features originating from the cavity mode and exciton, and show a very marked resonance behavior, with an enhancement in signal strength of more than an order of magnitude. In contrast, the corresponding R spectra show only a distinct cavity mode, and at best only a weak excitonic feature, and the resonance behavior is far less pronounced. Thus, our experiments indicate that PR has significant advantages over R spectroscopy, in that it detects both the cavity and excitonic modes, gives a measure of the degree of overlap, and, most importantly, yields a strongly enhanced signal when the modes are in close resonance. This last fact indicates that PR may be a very sensitive nondestructive room-temperature technique of great practical importance in VCSEL characterization, since it may be used to locate regions of the wafer where the resonance condition required for laser operation has been achieved.

We have also focused on developing an appropriate line shape model for fitting the VCSEL PR spectra in the vicinity of the cavity exciton resonance. As a starting point, this uses the same fundamental equation as the conventional PR model. However, there is a crucial conceptual difference: since the reflectance cavity mode originates from complicated interference effects between different layers in the structure, the Seraphin coefficients have sharp features rather than the more usual slowly varying functions of energy. By numerically calculating the Seraphin coefficients of the QW layers of the two VCSEL structures, we have established that, as a function of energy, they can be approximated by the real and imaginary parts of a complex Lorentzian. The modulation induced changes in the complex dielectric function of the QW are described by a conventional model, such as that based on first derivatives of a Lorentzian. Thus, the PR spectrum is represented by the product of two oscillatory line shapes which is quite different from the summation which occurs in conventional models, say for two excitonic transitions. This model has very different properties, especially when the two oscillators are close to resonance.

We have successfully fitted this line shape model to sets of position dependent PR spectra for the two samples, where essentially only one parameter is changing due to the growth fluctuations—the energy of the cavity mode. This satisfactorily reproduces not only the observed spectral line shapes, but also the strong enhancement of the PR signal near resonance. The fitted energy positions and linewidths of cavity mode and QW exciton indicate, at best, only a weak coupling between the cavity and the QW exciton, i.e., no anti-

crossing, or Rabi splitting, is unambiguously observed.

In summary, we have shown that PR spectroscopy, together with an appropriate line shape model, can provide a powerful tool for studying the exciton cavity coupling in semiconductor cavities such as VCSEL's and QMC's. In the following paper,[23] we introduce an application of PR to monitor both ground-state and higher-order excitonic transitions in QW's embedded in semiconductor cavities, based on the theory of PR line shapes developed here, and use this to study the resonance between these and the cavity mode.

## ACKNOWLEDGMENTS

*Electronic address: J. Hosea@surrey.ac.uk

[1] V. Savona, L. C. Andreani, P. Schwendimann, and A. Quattropani, Solid State Commun. **93**, 733 (1995).

[2] S. Jorda, Phys. Rev. B **50**, 18 690 (1994).

[3] A. Liu, Phys. Rev. B **55**, 7101 (1997).

[4] Y. Zhu, D. J. Gauthier, S. E. Morin, Q. Wu, H. J. Carmichael, and T. W. Mossberg, Phys. Rev. Lett. **64**, 2499 (1990).

[5] J. D. Berger, O. Lyngnes, H. M. Gibbs, G. Khitrova, T. R. Nelson, E. K. Lindmark, A. V. Kavokin, M. A. Kaliteevski, and V. V. Zapasskii, Phys. Rev. B **54**, 1975 (1996).

[6] J. Tignon, P. Voisin, J. Wainstain, C. Delalande, M. Voos, R. Houdré, U. Oesterle, and R. P. Stanley, Solid-State Electron. **40**, 497 (1996).

[7] C. Weisbuch, M. Nishioka, A. Ishikawa, and Y. Arakawa, Phys. Rev. Lett. **69**, 3314 (1992).

[8] T. A. Fisher, A. M. Afshar, D. M. Whittaker, M. S. Skolnick, J. S. Roberts, G. Hill, and M. A. Pate, Phys. Rev. B **51**, 2600 (1995).

[9] T. A. Fisher, A. M. Afshar, M. S. Skolnick, D. M. Whittaker, and J. S. Roberts, Phys. Rev. B **53**, R10 469 (1996).

[10] T. A. Fisher, A. M. Afshar, M. S. Skolnick, D. M. Whittaker, J. S. Roberts, G. Hill, and M. A. Pate, Solid-State Electron. **40**, 493 (1996).

[11] R. Houdré, C. Weisbuch, R. P. Stanley, U. Oesterle, P. Pellandini, and M. Ilegems, Phys. Rev. Lett. **73**, 2043 (1994).

[12] Z. L. Zhang, M. Nishioka, C. Weisbuch, and Y. Arakawa, Appl. Phys. Lett. **64**, 1068 (1994).

[13] R. Houdré, R. P. Stanley, U. Oesterle, M. Ilegems, and C. Weisbuch, Phys. Rev. B **49**, 16 761 (1994).

[14] P. Kelkar, V. Kozlov, H. Jeon, A. V. Nurmikko, C.-C. Chu, D. C. Grillo, J. Han, C. G. Hua, and R. L. Gunshor, Phys. Rev. B **52**, R5491 (1995).

[15] R. S. Geels, S. W. Corzine, and L. A. Coldren, IEEE J. Quantum Electron. **27**, 1359 (1991).

[16] R. S. Geels, B. J. Thibeault, S. W. Corzine, J. W. Scott, and L. A. Coldren, IEEE J. Quantum Electron. **29**, 2977 (1993).

[17] K. Bacher, B. Pezeshki, S. M. Lord, and J. S. Harris, Jr., Appl. Phys. Lett. **61**, 1387 (1992).

[18] D. H. Christensen, J. G. Pellegrino, R. K. Hickernell, S. M. Crochiere, C. A. Parsons, and R. S. Rai, J. Appl. Phys. **72**, 5982 (1992).

[19] J. Faist, J.-D. Ganière, P. Buffat, S. Sampson, and F.-K. Reinhart, J. Appl. Phys. **66**, 1023 (1989).

[20] P. D. Berger, C. Bru, T. Benyattou, G. Guillot, A. Chenevas-Paule, L. Couturier, and P. Grosse, Appl. Phys. Lett. **68**, 4 (1996).

[21] P. J. Klar, G. Rowland, T. E. Sale, T. J. C. Hosea, and R. Grey, Phys. Status Solidi A **170**, 145 (1998).

[22] O. J. Glembocki and B. V. Shanabrook, in *Semiconductors and Semimetals*, edited by R. K. Willardson and A. C. Beer (Academic Press, New York, 1989), Vol. 36, Chap. 4.

[23] P. J. Klar, G. Rowland, P. J. S. Thomas, A. Onischenko, T. E. Sale, T. J. C. Hosea, and R. Grey, Phys. Rev. B **59**, 2902 (1999).

[24] T. E. Sale, J. Woodhead, R. Grey, and P. N. Robson, IEEE Photonics Technol. Lett. **4**, 1192 (1992).

[25] B. O. Seraphin and N. Bottka, Phys. Rev. **145**, 628 (1966).

[26] J. E. Fisher and B. O. Seraphin, Solid State Commun. **5**, 973 (1967).

[27] T. J. C. Hosea, P. J. Hughes, and B. L. Wiess, J. Appl. Phys. **77**, 2672 (1995).

[28] T. J. C. Hosea, D. J. Hall, and R. T. Carline, J. Appl. Phys. **78**, 5084 (1995).

[29] B. V. Shanabrook, O. J. Glembocki, and W. T. Beard, Phys. Rev. B **35**, 2540 (1987).

[30] H. Shen, S. H. Pan, F. H. Pollak, M. Dutta, and T. R. AuCoin, Phys. Rev. B **36**, 9384 (1987).

[31] Y. S. Tang, J. Appl. Phys. **69**, 8298 (1991).

[32] P. J. Klar, C. M. Townsley, D. Wolverson, J. J. Davies, D. E. Ashenford, and B. Lunn, Semicond. Sci. Technol. **10**, 1568 (1995).

[33] D. E. Aspnes, Surf. Sci. **37**, 418 (1973).

[34] W. M. Theis, G. D. Saunders, C. E. Leak, K. K. Bajaj, and H. Morkoç, Phys. Rev. B **37**, 3042 (1988).